Table of Contents

1. Introduction to Infrared Spectroscopy

Infrared spectroscopy is a widely used method to characterize materials in gaseous, liquid, and solid state. Since almost all substances show distinctive absorption features in the infrared spectral region, it can be used to identify compounds as well as to investigate specific properties in a sample of known composition.

Examples for applications of infrared spectroscopy are:

- Concentration of impurities, dopant and trap concentration in anorganic semiconductors.
- Quantitative phase analysis.
- Phonon and lattice vibration energies.
- Molecular vibration energies.

Knowledge of these properties can, amongst other, be used to monitor

- Purity in industrial semiconductor fabrication.
- Internal stress, preferred orientation and other structural properties.

Just as in spectroscopy with visible light, the two classic experiments to determine a material's optical constants are to measure transmittance and reflectance. The only difference is the energy scale of the light that is used. Electromagnetic radiation of a wavelength below the visible (VIS) spectral range (~ *400 - 800 nm*) can be classified as follows:

- near infrared (NIR): *0.8 – 10 µm*
- mid(ddle) infrared (MIR): *10 – 40 µm*
- far infrared (FIR): *40 – 1000 µm*

From the two quantities that can be extracted from an infrared spectrum, the magnitude of the absorption (or reflectance or transmission) is mostly used to determine relative values. It is by far easier to conclude that this one sample has less impurities than the other or that the polymer chains in this one film are more oriented than in the other than to give absolute values. However, the energetic position of, for instance, an impurity vibration band in semiconductors can be determined in absolute values from the position of an absorption (transmittance, …) feature.

2. Light Sources, Detectors and Optical Components

Materials that are used for spectroscopy in the visible spectral range are often out of question for IR application, since their optical constants may be very different in the infrared. Consequently, new materials for lenses, mirrors, special coatings etc. had to be found. Because infrared spectroscopy is an important method in research as well as for industrial applications, a broad variety of light sources, optical components and detectors has been developed. A short overview will be given below.

2.1. Light Sources

2.1.1. Black Body Emitters

As in the visible spectral range standard radiation sources are black body emitters at high temperatures. Even though the maximum of the emitted intensity lies at (much) shorter wavelengths, the absolute amount of emission in the IR still increases about linearly with temperature. This can be illustrated when one takes into account that on one hand, according to Stefan-Boltzmann's law, the total energy E emitted from a black body scales as

$$E = \sigma \cdot T^4 \tag{1}$$

with temperature T and on the other hand, the spectral density of black body radiation can be described by Planck's law as follows:

$$E(\lambda) = \frac{2hc^2}{\lambda^5} \cdot \frac{1}{e^{\frac{hc}{\lambda k_B T}} - 1} \tag{2}$$

where h is Planck's constant, k_B Boltzmann's constant and c the speed of light. And additionally, for the wavelength λ_{max} at which the maximum intensity is emitted, we know from Wien's law that:

$$\lambda_{\max} \cdot T = const. = 2898 \mu m K \tag{3}$$

Note that from eq. (3) we can easily derive that a black body at room temperature (*300 K*) has a λ_{max} = *9.7 µm* which lies in the NIR (!). However the total intensity is negligible compared to the intensity of our IR light source. A few sample curves should illustrate this:

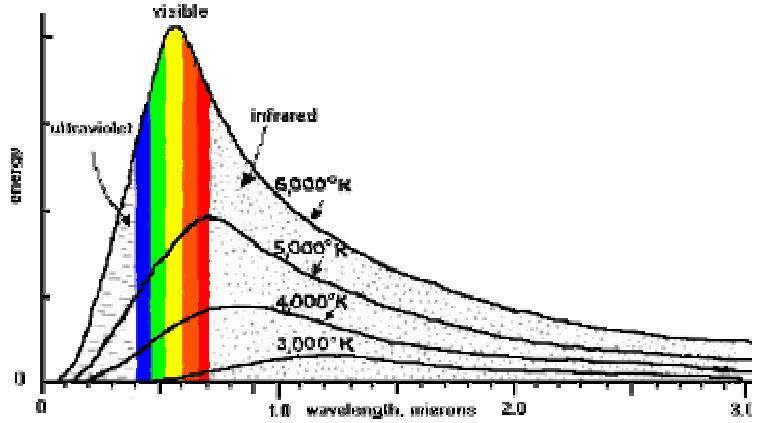

a)

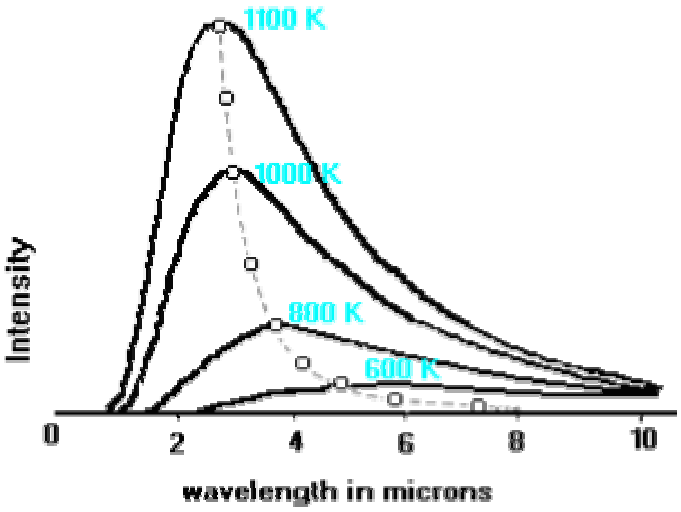

b)

Fig. 1: Planck curves for several temperatures of black body emitters.

A simple source operating on this principle is the "glowbar". As the name indicates, it consists of a SiC (or some ceramics) rod with the dimensions ~ *2 cm* length and ~ *0.5 cm* diameter, which is heated by about *5 A* to ~ *1450 K*. It is typically used in a spectral range down to *40 µm*. Because of its shape it can easily be imaged onto the entrance slit of a monochromator. The glowbar is operated in vacuum.

2.1.2. Plasma Sources

For more sophisticated applications in the FIR other sources must be used. Since the intensity at shorter wavelengths would be immense, if one wants to get black body radiation in the FIR at all, extensive filtering would be necessary. Hot gas plasmas emit a long wavelength continuum where, in the case of a totally ionized plasma, the intensity is independent of the wavelength. An example would be a high pressure mercury arc lamp.

2.1.3. IR Lasers

Although semiconductor lasers are not tunable over a sizable spectral range, they cover a wide spectrum not only in the NIR and MIR but also in the FIR, if suitably constructed. The advantage of a laser light source is quite obviously its high intensity, small beam divergence, coherence, etc. Despite the limited range of one single laser, many of them fall in the spectral range of the IR absorption lines of important gases (NO_2, SO_2, O_3, ….) an find broad application in environmental pollution control. Finally, the CO_2 Laser with an emission around 10 microns is one of the most powerful laser systems altogether. A schematic representation of the spectral range covered by a variety of semiconductor lasers together with the absorption lines of some important gases is depicted in Figure 2.

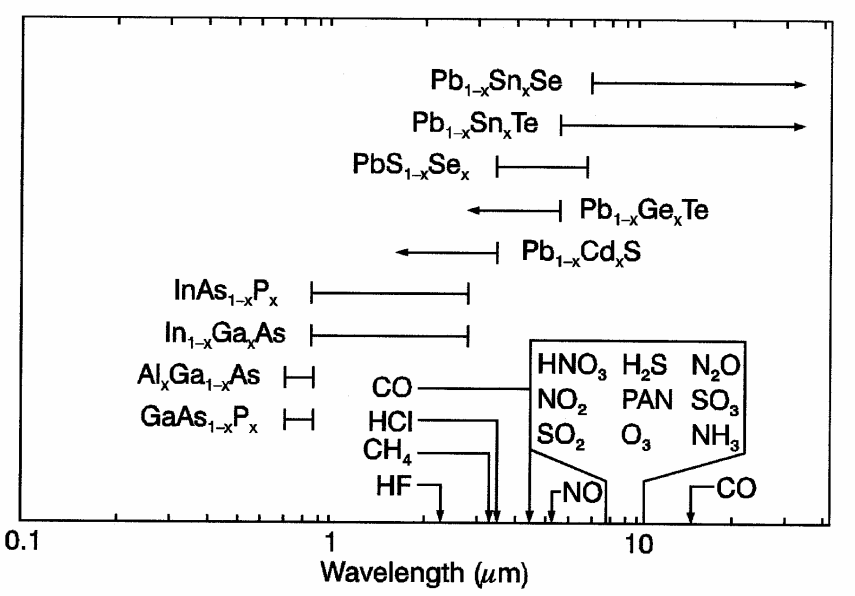

Fig. 2: The spectral range of IR Semiconductor Lasers.

2.2. Detectors

2.2.1. Photoconducting Detectors

Just as in the visible range, semiconductor detectors are used in the IR. Their common working principle is that electrons are excited into the conduction band by incident electromagnetic radiation. This is the same for two types of semiconductor detectors. Firstly, semiconductors are available with almost any desired bandgap. In that case, electrons are directly excited from the valence band and can contribute to the conductivity (PbS). Secondly, one could use a doped semiconductor (Ge:Cu, Ge:Zn or Ge:Ga) with the dopant levels close to either the valence or to the conduction band. Electrons are then excited from these levels into the conduction band or from the valence band into these levels. This would then result in a higher electron or hole conductivity respectively. Clearly one single semiconductor detector can not be used to cover the whole spectral range from the NIR to the FIR (up to ~ *150 µm*).

Because of the low light powers available and the relatively low sensitivity of the above mentioned detectors, especially in the FIR region, other detectors are frequently used.

2.2.2. Golay Detector

An often used system is the Golay Detector (Figure 3). It works on a pneumatic principle. Incident IR radiation is absorbed by a thin film. The film is heated and gives the heat in turn to a small gas volume confined into a chamber which the film seals. The other lid of the chamber is a thin mirror which images a grating onto itself in a simple optical setup. A small deviation from the overlap of object and grating then gives a signal to a detector. Obviously, the problem of detecting IR is up-converted to detecting VIS.

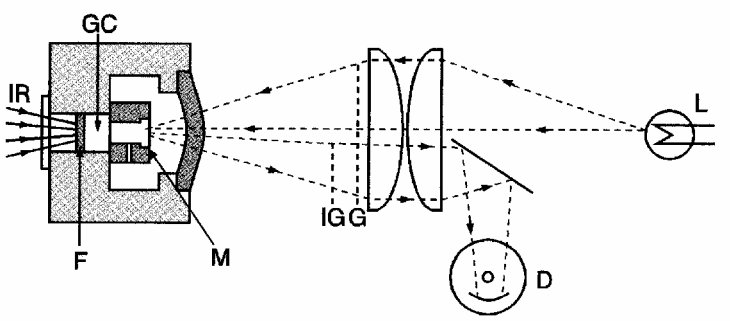

Fig. 3: Schematic Representation of a Golay Detector.

L . . . . . Light Source
D . . . . . Detector
G . . . . . Grating
IG. . . . . Image of the Grating
M . . . . . Mirror
GC. . . . . .Gas Chamber
F . . . . . .Absorbing Film
IR. . . . . Incident IR

This detector can be used up to *1000 µm*, but can only be employed for modulated (chopped) signals, best from *3* to *10 Hz*. So the instrument bandwith is very low.

2.2.3. Bolometers

More sophisticated but also more elaborate detectors are the low temperature Ge bolometers (Figure 4). They are based on the temperature induced change of the conductivity of a Ge crystal cooled to liquid Helium temperatures (*4.2 K*). IR radiation hits the Ge crystal through cold filters, used to reduce background radiation and heats it up. The conductivity is then measured over the voltage drop at a cooled resistance.

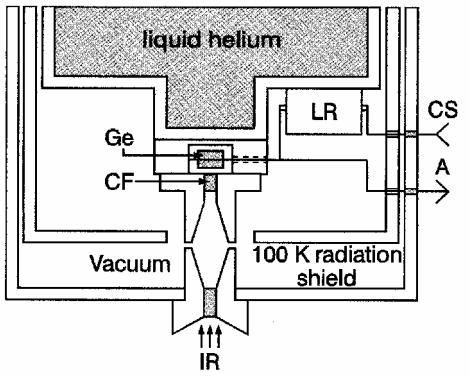

Fig. 4: A low temperature Ge bolometer.

CS . . . . . Current Supply
A . . . . . Amplifier
LR . . . . . Load Resistance
Ge . . . . . Ge Crystal
CF . . . . . Cold Filter
IR. . . . . Incident IR radiation

An often used dopant is Ga, which increases the sensitivity, but gives a rather low instrument bandwith of ~ *10 Hz*. Counterdoping with Sb slightly decreases the sensitivity but increase the bandwith to about *500 Hz*. In InSb based detectors, the strong temperature dependence of the charge carrier mobility rather than the carrier concentration is used to probe the heating of the detection crystal. They are called InSb-transformer detectors.

2.2.4. Pyroelectric Detectors

These detectors have a rather simple working principle. Crystals with a permanent electric dipole moment, react to a sudden change in the dipolar order with the generation of compensating charges. This disorder could be induced by an IR or heat pulse falling onto the crystal. The voltage induced by the generated compensating charges is then the detected quantity.

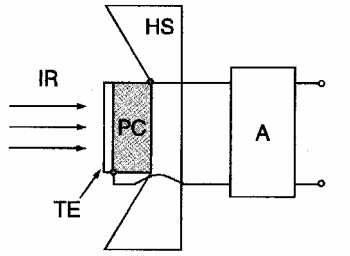

Fig. 5: Schematic arrangement of a pyroelectric detector.

A . . . . . Amplifier
HS . . . . . Heat Sink
PC . . . . . Pyroelectric Crystal
TE . . . . . Transparent Electrode
IR. . . . . Incident IR radiation

As can be seen from Figure 5, IR radiation falls through a transparent electrode onto the pyroelectric crystal, which is temperature stabilized on the other side via connection to a heat sink. This detector can be very fast with a rather high sensitivity. A well known crystal for this system would be triglycine sulfate (TGS).

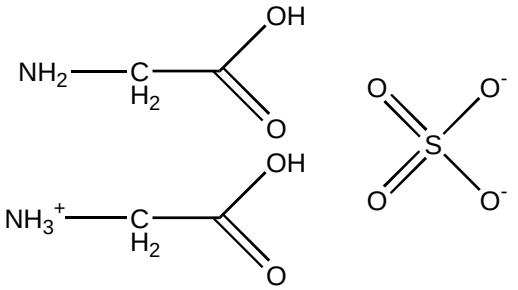

Fig. 6: Chemical structure of triglycine sulfate.

In some cases fully deuterated TGS is used (DTGS).

2.3. Optical Components

For any optical components like lenses, windows and filters, attention must be paid to the transmission properties of the materials. Many materials may appear transparent in the VIS spectral region but are opaque in the IR region and vice versa. In Figure 7 a listing of some materials used in IR spectroscopy together with their respective transmission range is shown.

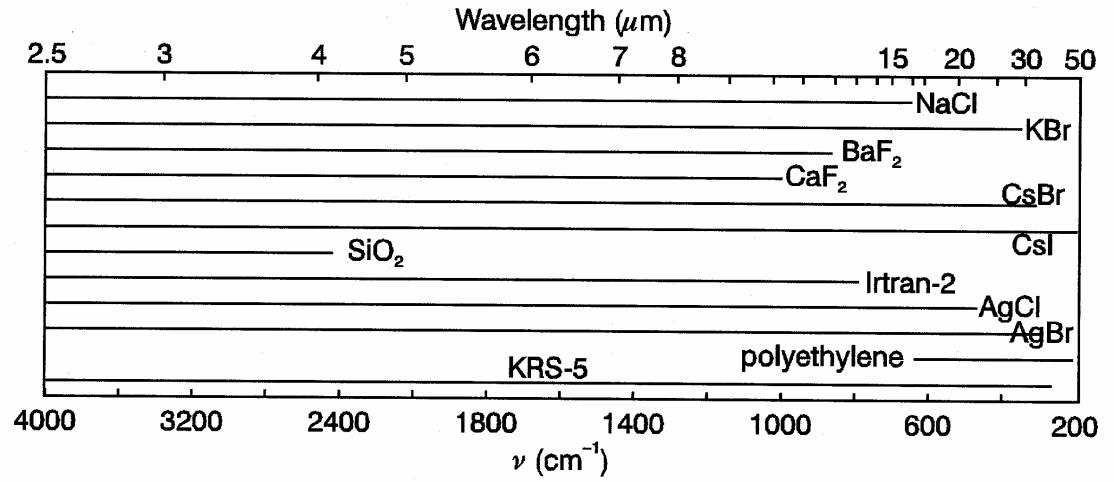

Fig. 7: Some materials used in IR spectroscopy and their transmission range.

In general one could say that the heavier the atomic components, the further in the IR the material can be used. However, due to its easy handling and industrial processability, polyethylene (PE) is widely used in FIR although it is only transparent down to ~ *15 μm*.

Any material where the transmission rapidly drops to zero at a given wavelength may be used as an edge filter. In the FIR, simple wire meshes will do, since they reflect light with a wavelength longer than the distance between the wires (see Figure 8).

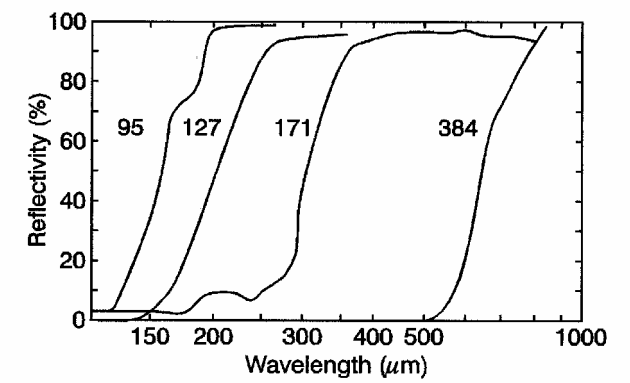

Fig. 8: Reflectance of wire mesh gratings. The numbers are the spacings in μm.

If one of the two components is omitted (only linear, parallel wires) these constructs may be used as polarizing filters with a very good extinction ratio.

3. FT-IR Spectroscopy

As with spectroscopy in the VIS spectral range, IR spectroscopy can be done by means of dispersive elements like prisms and gratings. However, several problems arise. Firstly, the available light intensities are very low. Secondly, a prism, if transparent in the IR at all, will generally have a very low dispersion in the red spectral region. Consequently, the remaining light intensity in a required window $\Delta\lambda$ is very low and hard to detect. Furthermore any one prism would not be sufficient for the whole spectral region from the NIR to the FIR.

As for (blased) gratings, the quality requirements may not be as high as for VIS spectroscopy, but other effects must be taken into account. Gratings for the FIR would require rather large spacings between the grid lines. Subsequently this would mean that to illuminate a sufficient amount of gridlines for a desired resolution, the gratings would have to be rather large.

3.1. Michelson Interferometer

A different approach, that uses not only a $\Delta\lambda$ window to generate a detector signal but the whole spectral range available from the light source and that does without any dispersive elements is interferometric spectroscopy.

The basic element of such a spectrometer is, besides a light source and a detector, a Michelson interferometer. Its components are shown in Figure 9.

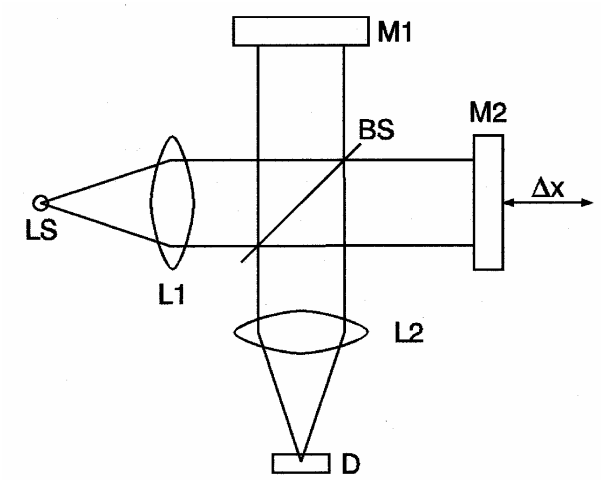

Fig. 9: Schematic representation of a Michelson interferometer.

LS. . . . . Light Source
L1. . . . . Collimating Lens
BS. . . . . Beam Splitter
M1. . . . . Fixed Mirror
M2. . . . . Moveable Mirror (Δx)
L2. . . . . Focusing Lens
D . . . . . Detector

Light from the light source is collimated an then split into two beams of equivalent intensity. The light is then reflected back onto itself by two planar mirrors. One of them is fixed, the other is linearly moveable over a distance Δx. The sample can conveniently only be placed in front of the Michelson interferometer. The light in the interferometer will create an interference pattern at the detector, that contains all the information about the light's spectral composition without using any dispersive elements. This means that all the available intensity is used for all wavelengths at once.

3.2. Fourier Transformation

Let the light coming from the light source be a plain wave after the collimating lens. The monochromatic electric field E_{inc}, after the beamsplitter can be written as:

$$E_{inc} = E_0^{'} \cdot e^{i(\omega t - kx)} \tag{4}$$

with $E^{'}_0$ being the amplitude, ω the frequency, k the wavevector and x the distance from the light source and t the passing time.

After being reflected by the fixed mirror on one hand and by the displaced mirror on the other hand, the total field at the detector E_D is given by:

$$E_D = \frac{1}{2} \cdot E_0 \left\{ e^{i[\omega t - kx]} + e^{i[\omega t - k(x+2\Delta x)]} \right\} \tag{5}$$

where $2\Delta x$ is obviously the optical path difference between the two interfering beams. We now let the detector rest at at $x = 0$ and rename Δx in x. The intensity I_D at the detector, which is proportional to the time-averaged square of the electric field is:

$$I_D(x) = const. \cdot \left\langle E_D^2 \right\rangle = const. \cdot \left(1 + e^{-i2kx}\right)^2 = const. \cdot \left(1 + \underbrace{2e^{-i2kx}}_{A} + \underbrace{e^{-i4kx}}_{B} \right) \tag{6}$$

In a next step, we neglect the faster oscillating and smaller term B in equation (6) and only keep term A. After the following manipulations:

$$k = \frac{2\pi}{\lambda} \qquad \text{and} \qquad c = \lambda \cdot \nu \qquad \text{gives} \qquad k = \frac{1}{c} \cdot 2\pi\nu \tag{7}$$

and forgetting about any constant factors, we find for the intensity at the detector introducing wavenumbers $\tilde{\nu} = \nu / c$:

$$I_D(x) = 1 + e^{-i4\pi\tilde{\nu}x} = \int_{-\infty}^{+\infty} d\tilde{\nu}' \cdot \delta\left(\tilde{\nu} - \tilde{\nu}'\right) \cdot \left[1 + e^{-i4\pi\tilde{\nu}'x}\right] = \int_{-\infty}^{+\infty} d\tilde{\nu}' \cdot I\left(\tilde{\nu}'\right) \cdot \left[1 + e^{-i4\pi\tilde{\nu}'x}\right] \tag{8}$$

when we write for the spectral density $I(\tilde{\nu}')$ of monochromatic light Dirac's delta distribution $\delta(\tilde{\nu} - \tilde{\nu}')$. However, equation (8) is true for any spectral density $I(\tilde{\nu}')$. If we split the integral on the right hand side in equation (8) into two parts, and assume that $I(\tilde{\nu}')$ drops sufficiently fast to zero for $\tilde{\nu}' \to \pm\infty$, we see that our interference pattern consists of a constant and an oscillating part:

$$I_D(x) = \int_{-\infty}^{+\infty} d\tilde{\nu}' \cdot I(\tilde{\nu}') + \int_{-\infty}^{+\infty} d\tilde{\nu}' \cdot I(\tilde{\nu}') \cdot e^{-i4\pi\tilde{\nu}'x} = I_0 + \int_{-\infty}^{+\infty} d\tilde{\nu}' \cdot I(\tilde{\nu}') \cdot e^{-i4\pi\tilde{\nu}'x} \qquad (9)$$

In fact, the remaining integral is the Fourier transformation of the spectral density.

Clearly, $I_D(x)$ reaches a maximum of $2I_0$ for $x = 0$, meaning zero optical path difference, and for large x any coherence is lost, the interference pattern converges to its mean value of I_0. In practice there are a few drawbacks from this theoretical description, that will be discussed in the next chapter.

3.3. Practical FT-IR

Since one is generally interested in the spectral density $I(\tilde{\nu}')$ and not in its Fourier transform $I(x)$, one has to perform a Fourier transformation on the recorded signal after registration. Nowadays this is done by a hardware implemented Fast Fourier Transformation (FFT). So the final output will be a:

$$I(\tilde{\nu}) = \int_{-\infty}^{+\infty} dx \cdot I(x) \cdot e^{i4\pi x\tilde{\nu}} \qquad (10)$$

From equation (10), we can immediately see the one problem will be the limits for the integration. Obviously we can not move the mirror from and to infinity but only over some finite distance. So instead of equation (10), we should rather write:

$$I(\tilde{\nu}) = \int_{x\min}^{x\max} dx \cdot I(x) \cdot e^{i4\pi x\tilde{\nu}} = \int_{-\infty}^{+\infty} dx \cdot \Theta(x - x_{\max}) \cdot \Theta(x_{\min} - x) \cdot I(x) \cdot e^{i4\pi x\tilde{\nu}} \qquad (11)$$

where $\Theta(x)$ is Heavyside's step function. This means that one should not simply take the Fourier transformation of the registered signal, but rather the Fourier Transformation of the recorded signal multiplied by a so called *apodization* function. Beside the rectangle function given in equation (11) a triangle function or other can be used.

Next, we will shortly discuss the question of resolution in a FT-IR setup. In order to be able to do this, the mechanism of data acquisition will be described shortly.

Firstly, for obvious practical reasons, the interference pattern at the detector will be registered by reading out the intensity in fixed time intervals corresponding to a certain displacement of the mirror Δx. How is this done? Along with the probing light, a collinear laser (typically HeNe) is sent through the Michelson interferometer. The laser interference pattern which, according to equation (8) is a simple cosine function, is recorded separately. At each zero of the laser interference pattern, a data point is sampled from the main beam (see Figure 10).

Secondly, as mentioned before, the data acquisition has to start and to stop at a specific position of the mirror. Usually the mirror is displaced periodically in order to get a whole series of interference patterns. Averaging will then give a better signal to noise ratio. To determine the starting point of one data acquisition run, the light from a broad band white light source is sent through the interferometer as well. This will give an interference pattern with a very sharp distinct peak at $\Delta x = 0$ (zero optical path difference), the so called center burst. This initializes every one data acquisition run.

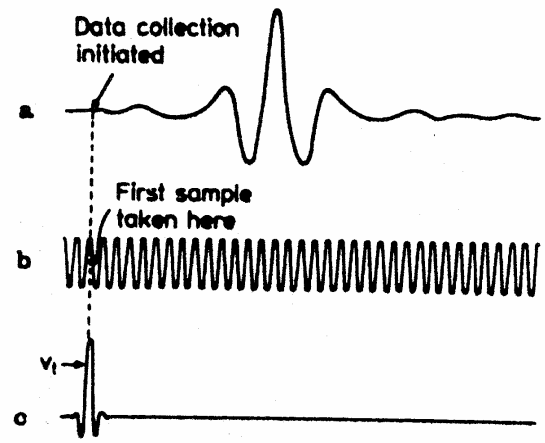

Fig. 10: Data collection mechanism in a FT-IR Michelson interferometer (a) sample beam, (b) laser interference pattern and (c) white light interference pattern (center burst)

How do these experimental boundaries affect our results? As can be seen from Figure (11) one needs at least two data points per period τ to correctly sample a simple sine function. Any signal with a period shorter than τ will not be detected.

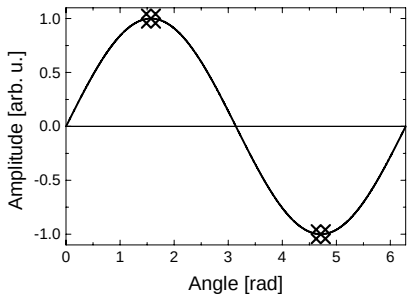

Fig. 11: Sine function (solid line) and the two necessary sampled data point (diamonds)

Finally, a longer data collection path (a longer total displacement of the mirror) means more orders of interference detected. Like in optics, this means a higher resolution in the wavenumber domain.

There are two important points to remember here:

- The sampling rate in space domain determines the high energy cut off in the wavenumber domain:

$$\tilde{\nu}_{\max} = \frac{1}{2\Delta x} \tag{12}$$

- The maximum displacement of the mirror limits the resolution in the wavenumber domain to:

$$\Delta\tilde{\nu} = \frac{1}{2x_{\max}} \tag{13}$$

4. Lab Exercises

We are now at a point where we can put all the things mentioned above to a practical use. This lab will try to give an overview over the applications of FT-IR spectroscopy.

4.1. Optical Constants of Silicon

As in ordinary VIS transmission spectroscopy, one will encounter interference patterns in the recorded spectrum, if the sample specimen has two polished, highly reflecting surfaces perpendicular to the probing beam. This pattern, that can be explained by a Fabry-Perot type interference (see Figure 12) will be superimposed on the actual transmission spectrum. In a spectral region, where no fundamental excitations are lying, this interference pattern can be extracted separately (given the instrument resolution is high enough) and used for other purposes.

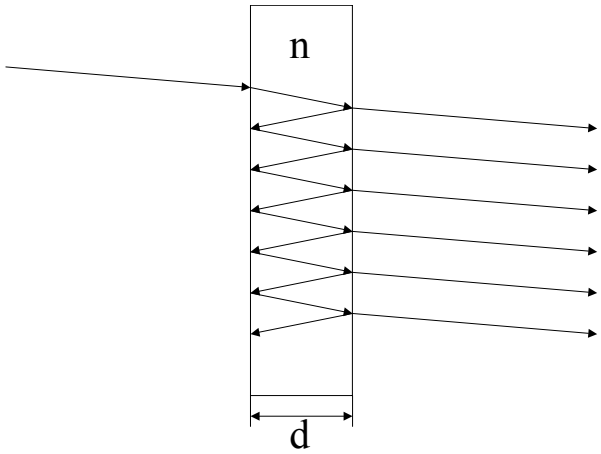

Fig. 12: Fabry-Perot Interference in a thin slab (thickness *d*) with refractive index *n*.

All the transmitted waves resulting from multiple internal reflection of the incident beam will interfere with each other. For normal incidence, the condition for constructive interference is met when the optical path difference between two partial beams is a multiple of the light's wavelength:

$$i \cdot \lambda = 2 \cdot n \cdot d \tag{14}$$

with $i = 1, 2, 3, \ldots$ while the destructive interference occurs when:

$$(2i+1) \cdot \frac{\lambda}{2} = 2 \cdot n \cdot d \tag{15}$$

The objective of this part of the lab is to determine the refractive index of silicon in a given spectral region in the infrared. Note that the generally complex refractive index n is only real if the material is an isolator and no absorption occurs.

4.2. Impurities in Silicon

To ensure high charge carrier mobility and thus high efficiency of silicon based integrated circuits, it is very important to introduce a minimum of impurities during fabrication. At least one needs a method to quantify the amount of impurities.

During the crystal growth process, oxygen impurity is easily incorporated into the silicon crystal, mainly from the air surrounding the melt. The oxygen atoms occupy interstitial sites in the silicon unit cell (see Figure 13) and form two strong Si-O bonds with the nearest neighbor silicon atoms.

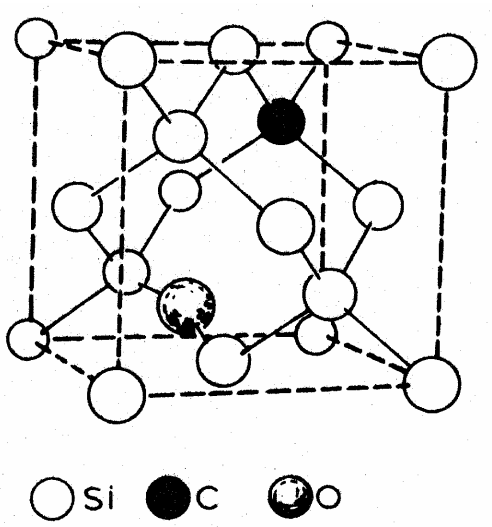

Fig. 13: Silicon unit cell with interstitial carbon and substitutional oxygen.

Carbon impurity can be introduced into the silicon crystal from the crucibles used in the crystal growth process. Carbon, being tetravalent too, can occupy lattice sites normally occupied by a silicon atom. It sits on a substitutional site.

Silicon itself, being a semiconductor will be transparent in the IR region apart from absorption bands due to phonons. Of course the introduction of local defects (C and O atoms) will lead to different force constants between the involved atoms and thus to different vibrational frequencies of the involved phonons. So each impurity will have its characteristic absorption band, whose absorption coefficient can be used for quantitative determination of impurity content.

To identify and measure absorption bands of impurities, one needs first of all a high-purity silicon single crystal reference, as can be produced by float zone (FZ) processing of a CZ crystal. The difference in the IR absorption can be seen from Figure 14.

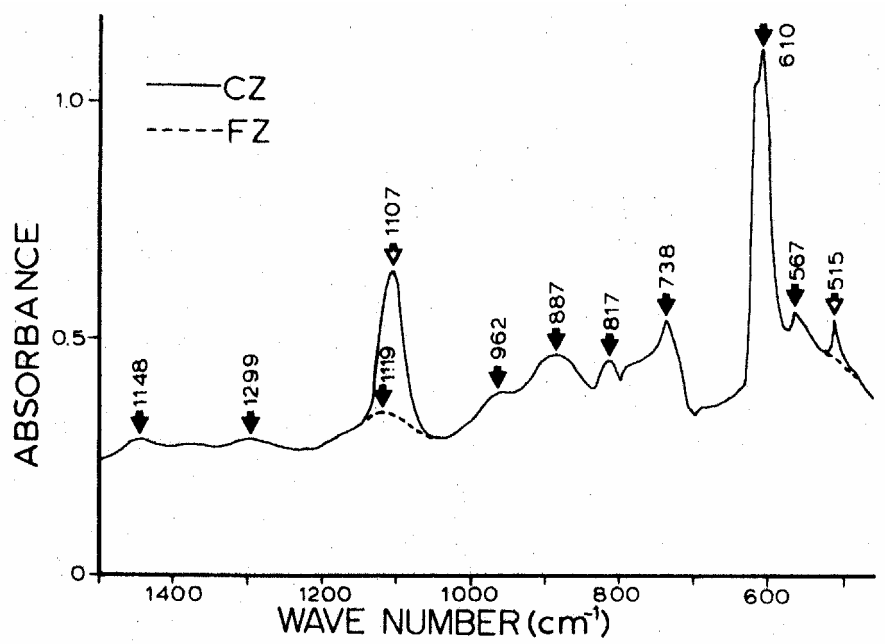

Fig. 14: IR absorption spectrum of silicon (CZ) and high purity silicon (FZ).

The band frequencies of FZ Silicon and their absorption coefficient are listed in Table I.

Table I: Band frequencies and absorption coefficients of FZ silicon.

Band frequency [cm^{-1}]	Absorption coefficient [cm^{-1}]
566	2.79
610	9.29
739	2.84
819	1.93
886	2.17
960	1.35
1118	1.04
1299	0.40
1448	0.44

If we subtract the two curves shown in Figure 14 from each other, the difference spectrum will show the vibrational phonon bands due to impurities only (see Figure 15).

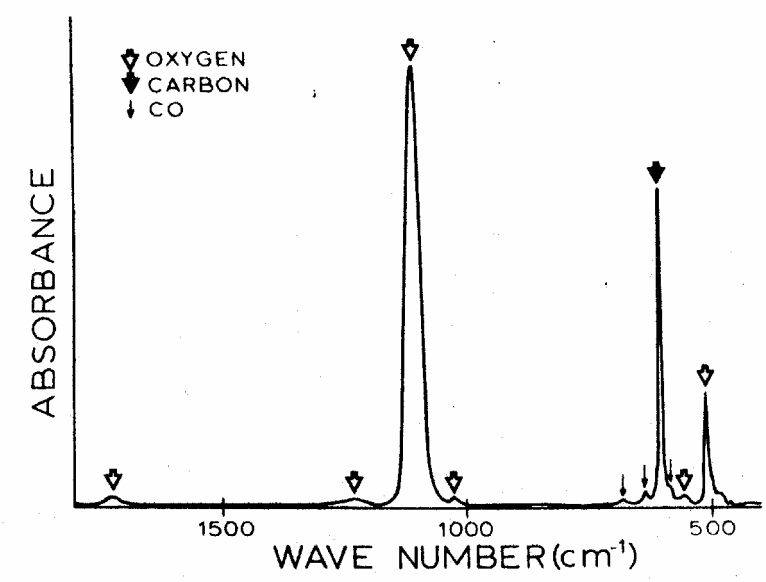

Fig. 15: Difference spectrum CZ-FZ showing the impurity phonon absorption bands only.

The oxygen bands have been interpreted in terms of an almost linear Si-O-Si quasi-molecule. The three fundamental vibrations of this moiety are a symmetric stretching (ν_1), an asymmetric stretching (ν_2) and a symmetric bending (ν_3). The band assignment of the oxygen impurities is listed in

Table II: Characteristic IR signature of interstitial Oxygen impurities in Silicon.

Frequency [cm^{-1}]	FWHM [cm^{-1}]	Relative Intensity	Assignment
515	8	0.260	ν_1
1013	8	0.006	$2 \times \nu_1$
1107	33	1.000	ν_2
1720	31	0.016	$\nu_1 + \nu_2$

In this exercise we will measure different Si wafers and try to determine the amount of oxygen impurity in them. Band assignment of all the absorption bands seen in pristine silicon and with implanted impurities is still incomplete and will not be topic of this lab.

4.3. Molecular Crystals

Another important application of IR spectroscopy is chemistry. Many molecules show distinctive absorption bands in the IR that are due to their normal vibrations whose energy levels lie in that spectral region.

The characteristic frequencies are indicative for bond orders, specific sidegroups etc. and can help to identify a substance, to monitor the outcome of a chemical synthesis or to probe the local environment of a certain molecule or sidegroup.

In this part of the lab we will try to record the IR-transmittance spectrum of simple organic molecules, using different sample preparation techniques, and to assign the molecular vibration bands.

Typical samples would be polycrystalline powders of *p*-quaterphenyl, *p*-terphenyl, *p*-sexiphenyl and fluorene.

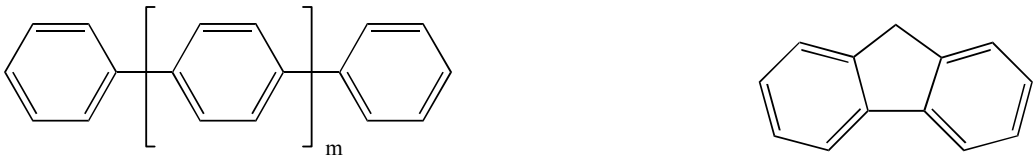

a) b)

Fig. 16: Chemical structure of oligo(*p*-phenylenes) (a) and fluorene (b).

Since all this substances are more or less soluble, one possibility of sample preparation would be to grow a film from solution on a suitable substrate. However, the crystallites might grow in a preferred orientation. To amend for this possible anisotropy one would have to make sure that the crystallites are evenly orientated in space. This could be achieved by either preparing a solid or a liquid solution with a suitable solvent.

4.4. Polymer Films

In this final part of the lab, the polarized IR-transmittance of an isotropic and an oriented polyethylene film will be studied.

The chemical structure of polyethylene (PE) is given in Figure 17. In an isotropic sample, the polymer chains will be running in every direction, all curled up. Statistically the number of chains in any direction perpendicular to the probing beam will be equal and consequently any orientational effects will average out.

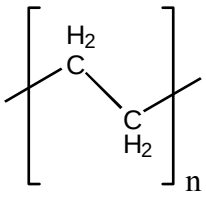

Fig. 17: Chemical structure of all trans polyethylene.

However, if we introduce a preferred orientation in the film by simple mechanical stress, the chains will be stretched out and lie preferably in one direction. This will show up in the difference between parallel and perpendicular polarized transmission spectra.

In fact, this very procedure is used in monitoring a polymer film's quality during industrial manufacturing.

5. Calculating Frequencies, Normal Modes and Intensities

In this chapter the theoretical aspects of describing the internal degrees of freedom of a bound ensemble of atoms will shortly be discussed. Only a classical treatment will be introduced, the quantum mechanical notion will be commented on without derivation.

5.1. The Harmonic Oscillator

Let us consider the problem of two masses m_n, $n = 1, 2$ connected to each other with a spring that is following Hook's law. That means that the acting force F is proportional to the deviation x' of the distance between the masses from some equilibrium distance x_0:

$$F = -k'' \cdot \left(x' - x_0\right) \tag{16}$$

where k'' is the force constant. Obviously, the only interesting coordinate for describing the internal degree of freedom of this system is the distance between the masses, the normal coordinate, and not the coordinates in space of the masses themselves. Furthermore, the constant equilibrium distance is not important to describe the dynamics and the energy of this system. We could go to the normal displacement $x = (x' - x_0)$ instead. The solution to this problem is of course a harmonic motion of the form:

$$x(t) = A_0 . \cos(\omega t + \varphi) \tag{17}$$

where A_0 is the amplitude of the motion, the maximum displacement, φ is some phase shift that accounts for the choice of $x(t = 0)$ and $\omega = \sqrt{\frac{k''}{\mu}}$ where we introduced the reduced mass $\mu = \frac{m_1 \cdot m_2}{m_1 + m_2}$.

Note that the corresponding potential energy function V would then be:

$$V = \frac{1}{2} \cdot k'' \cdot \left(x' - x_0\right)^2 = \frac{1}{2} \cdot k'' \cdot x^2 \tag{18}$$

5.2. Coupled Harmonic Oscillators

Let us now consider an ensemble of N particles with masses m_n, $n = 1, 2, \ldots, N$ with harmonic forces (see equation (16)) between each of them. Naturally one needs $3N$ coordinates, cartesian or other, to describe the positions of these particles. Following

equation (18) we will now expand the potential energy function V in a taylor series over the displacements of the $3N$ positions from the equilibrium positions:

$$V = V_0 + \sum_{i=1}^{3N} \left(\frac{\partial V}{\partial x_i} \right)_{x_i=0} \cdot x_i + \sum_{i=1}^{3N} \sum_{j=1}^{3N} \frac{1}{2!} \left(\frac{\partial^2 V}{\partial x_i \partial x_j} \right)_{x_i, x_j=0} \cdot x_i \cdot x_j + O\left(x^3\right) \tag{19}$$

We can always chose $V_0 = 0$, $\left(\frac{\partial V}{\partial x_i} \right)_{x_i=0} = 0$ because this is how an equilibrium position is defined and in harmonic approximation terms of order x^3 and higher will be neglected. The derivations in the brackets are nothing more than the force constants k''_{ij}. Instead of introducing reduced masses, we will go from Cartesian displacements x_i to mass weighted Cartesian displacements q_i by setting $q_i = \sqrt{m_i} \cdot x_i$, where $m_{i=3n} = m_{i=3n-1} = m_{i=3n-2}$. Equation (19) will then become:

$$V = \sum_{i=1}^{3N} \sum_{j=1}^{3N} \frac{1}{2} k'_{ij} q_i q_j \tag{20}$$

where $k'_{ij} = \frac{k''_{ij}}{\sqrt{m_i m_j}}$. The total energy (kinetic and potential) of the system, which corresponds to the Hamilton function H in conservative systems, would then look like:

$$H = \sum_{i=1}^{3N} \frac{1}{2} p_i^2 + \sum_{i=1}^{3N} \sum_{j=1}^{3N} \frac{1}{2} k'_{ij} q_i q_j \tag{21}$$

where p_i is the mass weighted momentum.

When deducing the equations of motion from this Hamiltonian by applying the Euler-Lagrange equations, one finds a set of $3N$ simultaneous second order linear differential equations for the q_is, yielding $3N$ sets of solutions that are of the expected (eq. 17) form:

$$q_i(t) = A_i \cos\left(\omega_j t + \varphi_i\right) \tag{22}$$

where i is the index for the $3N$ coordinates and j is the index for the $3N$ solutions. Inserting this ansatz in the equations of motion leads to an eigenvalue problem of the $3N \times 3N$ matrix k'_{ij} with $3N$ eigenvalues k_j and $3N$ eigenvectors A_{ij}. Since there are only $3N$-6 internal degrees of freedom, 6 k_js will be zero and the corresponding A_{ij} will be three translations and three rotations of the whole ensemble.

A solution j with its phase factors φ_i set to one common value and normalized Amplitudes A_i is called a normal mode of the ensemble with its characteristic

eigenfrequency ω_j. Any complex motion of the system can be described as a superposition of its normal modes.

5.3. Intensities and Selection Rules

Let us now assume that for an ensemble of quantum mechanical particles such as the atoms in a molecule or in a solid the total energy as well as the energy in each of the normal modes can only take on discrete values.

$$E_{tot} = \sum_{j=1}^{3N} \hbar\omega_j \left(\nu_j + \frac{d_j}{2} \right) \tag{23}$$

Here, ν_j is the occupation number of mode j and d_j its degeneracy. Since the energy difference $\hbar\omega_j$ between two energy levels of such a mode, typically the ground an first excited state, is often in the IR, this is, what we will see in our spectrum (see Figure 18).

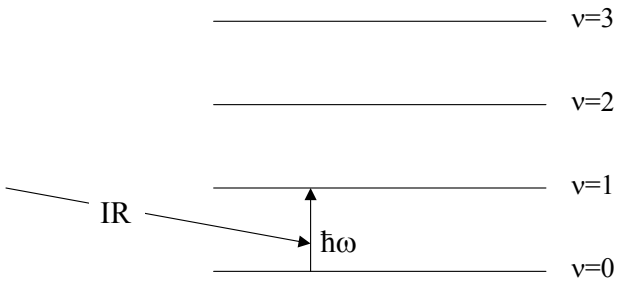

Fig. 18: Infrared absorption process from the ground to the first excited state.

Let a system as depicted in Figure 18 vibrate in the ground state of one normal mode (or of many; they can be treated as completely independent within harmonic approximation) with a certain frequency ω_j. Let us suppose, that during that oscillation around some equilibrium position, the intrinsic dipole moment of the system oscillates with this very frequency around some equilibrium value (zero or other). Now we switch on a light beam with frequency ω_0 and let it fall on this system. The external electric field will polarize the electron cloud and induce an additional dipole moment. The situation now corresponds to an externally driven harmonic oscillator. When ω_0 coincides with ω_j, the system will be in resonance with the external driving force and will take up energy → it will absorb an IR photon and jump to next highest energy level.

In the language of quantum mechanics, the condition that an oscillation corresponding to the normal mode of the system changes its dipole moment, means that the transition dipole matrix element between the initial state ν_i and the final state ν_f must be non-zero:

$$\left\langle \nu_i \middle| \hat{\mu} \middle| \nu_f \right\rangle \neq 0 \tag{24}$$

where $\hat{\mu} = -e\hat{R}$ is the electric dipole moment operator and $\hat{R}$ the position operator. We will now expand the dipole moment in a Taylor series over the normal coordinate (the coordinate along which the atoms are displaced during a normal vibration) Q_j of a vibration j:

$$\mu = \mu_0 + \frac{\partial \mu}{\partial Q_j} \cdot Q_j + ... \qquad \hat{\mu} = \mu_0 + \frac{\partial \mu}{\partial Q_j} \cdot \hat{Q}_j + ... \tag{25}$$

Inserting equation (25) into equation (24) yields:

$$\frac{\partial \mu}{\partial Q_j} \cdot \left\langle \nu_i \middle| \hat{Q}_j \middle| \nu_j \right\rangle \propto \frac{\partial \mu}{\partial Q_j} \cdot \left\langle \nu_i \middle| \hat{a} - \hat{a}^+ \middle| \nu_j \right\rangle \tag{26}$$

Where $\hat{a}$ and $\hat{a}^+$ are the step operators of the harmonic oscillator. From equation (26) one can see that the matrix element is only non-zero if $\left| \nu_{final} \right\rangle = \left| \nu_{initial} \pm 1 \right\rangle$ corresponding to an IR absorption or emission process between two adjacent levels (see Figure 18). One could also write this important selection rule as:

$$\Delta \nu = \pm 1 \tag{27}$$

According to Fermi's golden rule, the absorption coefficient α_j corresponding to such a process is proportional to the square of the matrix element:

$$\alpha_j \propto \left| \left\langle \nu_i \middle| \hat{\mu} \middle| \nu_f \right\rangle \right|^2 \propto \left| \frac{\partial \mu}{\partial Q_j} \right|^2 \tag{28}$$

Computing the right hand side of equation (28) to predict IR intensities is a challenge to quantum chemists even today.

6. Bibliography

H. Kuzmany, “Solid State Spectroscopy”, *Springer Verlag Berlin Heidelberg New York (*1998).

H. Kuzmany, “Festkörperspektroskopie”, *Springer Verlag Berlin Heidelberg New York (*1990).

E. B. Wilson jr., J. C. Decius and P. C. Cross, “Molecular Vibrations”, *Dover Publications Inc. New York* (1980).

C. Weißmantel and C. Hamann, “Grundlagen der Festkörperphysik“, *Springer Verlag Berlin Heidelberg New York* (1980).

Bergmann and Schaefer, “Lehrbuch der Experimentalphysik, Band 3: Optik“, *Walter de Gruyter Berlin New York* (1993).

D. O. Hummel, “Polymer Spectroscopy, Monographs in Modern Chemistry Vol. 6”, *Verlag Chemie* (1974).

7. Annexes

7.1. Annex I: BOMEM FT-IR Spectrometer MB102

In this Annex will give some details on the spectrometer used for the lab. Please refer also to the attached photocopies.

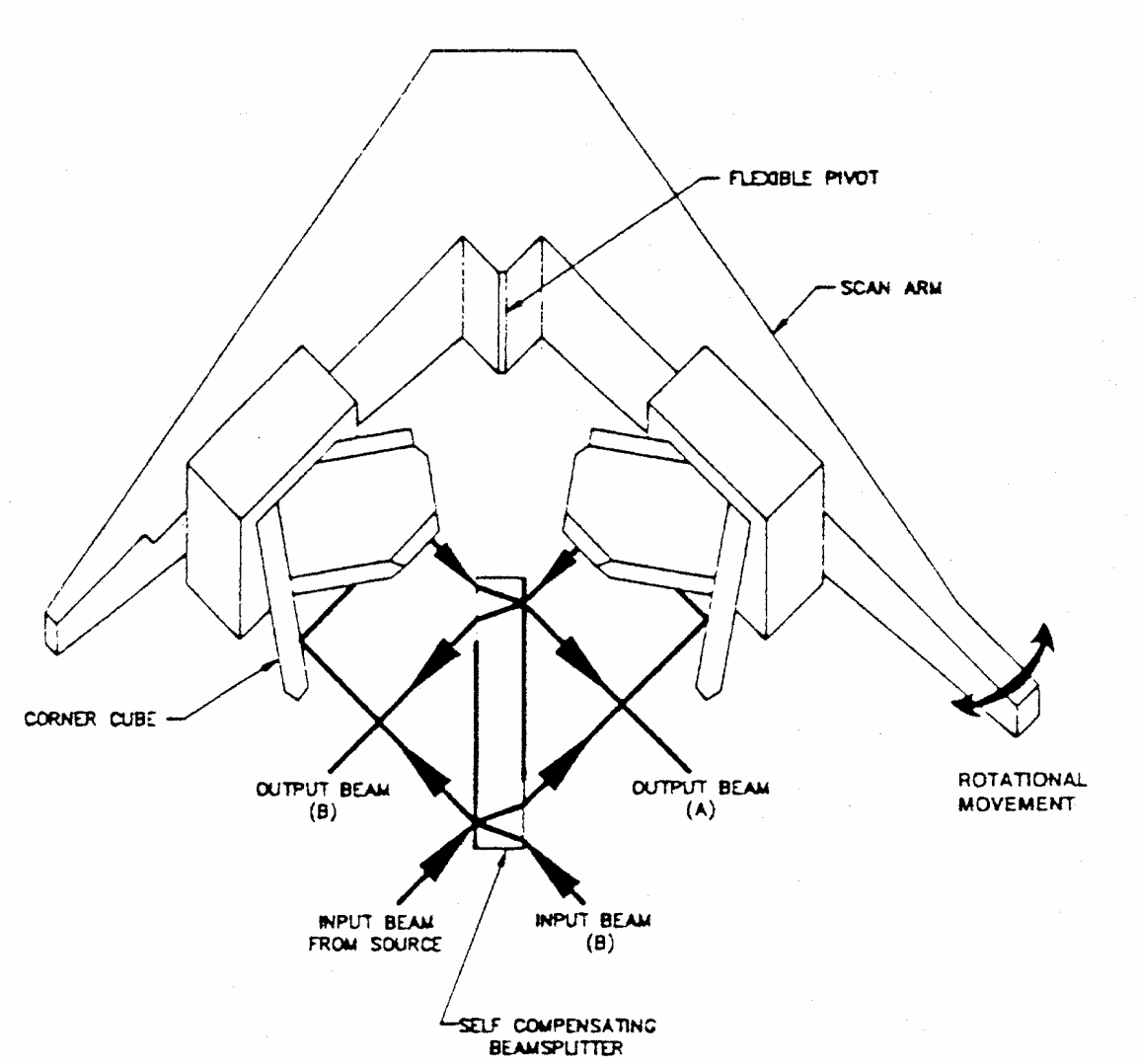

Fig. 19: The wishbone scanning type Michelson interferometer in the BOMEM MB series FT-IR spectrometers.

7.2. Annex II: IR spectra of some organic compounds

The following spectra (see attached photocopies) are taken from: C. J. Pouchert, "The Aldrich Library of Infrared Spectra", *Aldrich Chemical Company Inc.* **3rd Edition**, 1981. They might prove useful for the analysis of the data recorded during the lab exrcises.